First published in: Continuum scale simulation of engineering materials. Weinheim, 2004.
ISBN 3-527-30760-5

14 Motion of Multiple Interfaces: Grain Growth and Coarsening

Britta Nestler

A new diffuse interface model (phase-field model) for non-isothermal solidification in alloy systems with multiple components and multiple phases is introduced. The model is capable to describe phase transitions, microstructure formations and interfacial motion in polycrystalline grain structures. The model is derived from an entropy functional in a thermodynamically consistent way and is related to classical sharp interface models in the limit of zero interface thickness. Anisotropic and facetted growth characteristics are included in both the kinetic coefficients and the surface energies. The set of governing equations is discretized and implemented. 2D and 3D simulations are performed showing the temporal evolution of phase fractions combined with the heat and mass diffusion during solidification and melting processes. To improve the computational efficiency for large domains, two strategies are followed. Firstly, a 3D parallel simulator based on a heterogeneous network of workstations is set up. This network solves the governing equations using a finite difference discretization on a uniform grid with explicit time update. Secondly, an adaptive finite element differential equation analysis library is used. Simulation results are presented showing the motion of multiple interfaces (phase and grain boundaries). In particular, phenomena such as anisotropic and crystalline curvature flow, grain growth, coarsening, wetting, symmetry properties and stability conditions of adjacent multiple junctions are described. In order to describe phase transformations and solidification processes in multi-component alloys, the specific phase diagrams are incorporated in the diffuse interface model via the free energies. Within this context, ternary eutectic structures are simulated. The effect of anisotropy on eutectic structures, such as the growth of tilted eutectic lamellae, and the formation of eutectic grains at different length scales: the grain structure on a larger scale and the eutectic substructure on a smaller scale are investigated. The stability of ternary eutectic growth fronts and the characteristic spacings depending on process conditions are studied by iterated simulations.

14.1 Introduction

The phase-field method has become a powerful methodology to describe phase transition phenomena in alloys with reliable qualitative results in comparison with experimental data. The method has successfully been used to describe solidification processes (e.g. Caginalp et al. (1989); Penrose and Fife (1990); Karma and Rappel (1998); Karma (2001)) as well as microstructure evolution in solids (e.g. Fried and Gurtin (1994)) and liquid-liquid interfaces (e.g. Lowengrub and Truskinovsky (1998)). Diffuse interface models have been formulated

Continuum Scale Simulation of Engineering Materials: Fundamentals – Microstructures – Process Applications.
Edited by Dierk Raabe, Franz Roters, Frédéric Barlat, Long-Qing Chen

ISBN: 3-527-30760-5

for pure substances (e.g. Caginalp et al. (1989); Penrose and Fife (1990)), binary alloys (e.g. Caginalp and Xie (1998); Tiaden et al. (1998)) for eutectic, peritectic and monotectic systems (e.g. Wheeler et al. (1996); Nestler and Wheeler (2000); Nestler et al. (2003, 2000); Plapp and Karma (2002)). Furthermore the evolution of grain boundaries can be modelled by phase-field approaches or order parameter models (e.g. Chen and Yang (1994); Fan and Chen (1997); Garcke and Nestler (2000); Nestler and Wheeler (1998)). The concept of describing interface evolution by a phase-field model was originally introduced by Langer (1986) using ideas of Halperin et al. (1974) who studied critical exponents for transport coefficients. Diffuse interface models such as the phase-field model have the characteristic property that the interfaces in the system have a non–zero thickness. First approaches of diffuse interfaces were already used by van der Waals (1893); Cahn and Hilliard (1958) and Landau and Ginzburg (1965). In papers by Caginalp and Fife (1988); Caginalp et al. (1989), the authors carried out a formal asymptotic expansion for phase-field models of solidification. By taking the limit of vanishing interfacial thickness, the diffuse interface profile relates to classical sharp interface models, also known as Stefan problems where the interface is described by a sharp step function profile. In these sharp interface models, boundary conditions for the physical quantities have to be prescribed at the interface between two bulk phases. In recent years, phase-field models have been derived from thermodynamic principles being now referred to as thermodynamically consistent (see Penrose and Fife (1990); Wang et al. (1993)).

Traditionally, the evolution of interfaces has been modelled by moving free boundary problems separating the regions of pure phases by a sharp interface contour line. In these sharp interface models, partial differential equations for e.g. mass and heat diffusion are solved within the bulk phases. These equations are coupled by boundary conditions on the interface, such as the Stefan condition demanding energy balance and the Gibbs-Thomson equation. Across the sharp interface, quantities such as the heat flux, the concentration field and the energy may show a discontinuous jump profile. The physics at the boundaries is prescribed by explicit tracking of the interfaces. In diffuse interface models the different bulk phases in the system are distinguished by a vector of phase-field variables ϕ_α. The number of components of this vector depends on the number of phases or grains of different crystal structure or orientation in the system. The phase boundaries are modelled by a diffuse interface, where the phase fields and other physical quantities change smoothly on a thin transition layer. For a single solid-liquid phase transition, the phase-field variable ϕ may take values of one in the solid and zero in the liquid. Across the interface, the phase field varies smoothly from one to zero. From a computational point of view, it is required that the spatial resolution of the numerical method must be finer than the thickness of the diffuse phase boundary layer. The interfacial thickness itself must be less than the characteristic scale of the growing microstructure. In this case, a nonuniform grid with adaptive refinement can dramatically reduce computational resources compared with a uniform grid with the same spatial resolution.

In the following sections a non-isothermal phase-field model is derived in a thermodynamically consistent way that allows for an arbitrary number of phases/grains and components and that is defined solely via the bulk free energies of the individual phases, the surface energy densities of the interfaces and diffusion and mobility coefficients. Since the diffuse interface model yields classical moving boundary problems in the sharp interface limit, the full set of phase-field evolution equations is defined by quantities which can experimentally be measured. The physical effects occurring during the solidification such as heat and mass transfer,

the release of latent heat, solute trapping, the Gibbs-Thomson relation and interface kinetics are obtained on the basis of an entropy functional. Since the bulk free energies determine the phase diagrams (see e.g. Chalmers (1977); Haasen (1994)), the new model is applied to phase transitions for arbitrary phase diagrams.

First, the diffuse interface model is introduced in its full generality, the free energy contributions are defined and the equations driving the phase evolution, heat and mass transfers in the system are derived. Then the numerical method for solving the governing equations is explained and 2D and 3D simulations of moving grain and phase boundaries are presented. In particular, simulations of grain growth, coarsening and microstructure formations in ternary alloys with different surface energy anisotropies are shown.

14.2 The Diffuse Interface Model

The diffuse interface model for a general class of alloy systems is formulated consisting of K components $(Al, Fe, Si, Cu, \ldots)$ and N different phases and grains of different crystal structures and orientations in a domain $\Omega \subset \mathbf{R}^3$. The concentrations and phase fractions or grains are represented by a vector $\boldsymbol{c}(\vec{x},t) = (c_1(\vec{x},t), \ldots, c_K(\vec{x},t))$ and by an order parameter $\boldsymbol{\phi}(\vec{x},t) = (\phi_1(\vec{x},t), \ldots, \phi_N(\vec{x},t))$, respectively. The phase-field model is based on an entropy functional of the form

$$S(e, \boldsymbol{c}, \boldsymbol{\phi}) = \int_\Omega \left(s(e, \boldsymbol{c}, \boldsymbol{\phi}) - \left(\varepsilon a(\boldsymbol{\phi}, \nabla\boldsymbol{\phi}) + \tfrac{1}{\varepsilon} w(\boldsymbol{\phi}) \right) \right) dx. \tag{14.1}$$

The bulk entropy density s is assumed to depend on the internal energy density e, on the concentrations of the components c_i, $i = 1, \ldots K$, and on the phase-field variable $\phi_\alpha, \alpha = 1 \ldots N$. The additional contributions $a(\boldsymbol{\phi}, \nabla\boldsymbol{\phi})$ and $w(\boldsymbol{\phi})$ of the entropy functional reflect the thermodynamics of the interfaces (e.g. Visintin (1996)). In diffuse interface models, ε is a small length scale parameter related to the thickness of the diffuse interface. The surface entropy contributions are expressed by a Ginzburg-Landau type functional of the form

$$-\int_\Omega \left(\varepsilon a(\boldsymbol{\phi}, \nabla\boldsymbol{\phi}) + \tfrac{1}{\varepsilon} w(\boldsymbol{\phi}) \right) dx,$$

where $a(\boldsymbol{\phi}, \nabla\boldsymbol{\phi})$ is a gradient energy density and $w(\boldsymbol{\phi})$ is an energy of multi-well or multi-obstacle type. Examples of possible choices will be given in the next section. The variable ϕ_α denotes the local fraction of phase α and it is required that the concentrations of the components and the phase-field variables fulfill the constraints

$$\sum_{i=1}^{K} c_i = 1, \qquad \sum_{\alpha=1}^{N} \phi_\alpha = 1. \tag{14.2}$$

It will be convenient to use the free energy as a thermodynamical potential. Therefore the Gibbs relation is postulated

$$df = -s dT + \sum_i \mu_i dc_i + \sum_\alpha r_\alpha d\phi_\alpha,$$

where T is the temperature, $\mu_i = f_{,c_i}$ are the chemical potentials and $r_\alpha = f_{,\phi_\alpha}$ are potentials due to the appearance of different phases. The notations $f_{,c_i}$ and $f_{,\phi_\alpha}$ denote the partial derivatives of the free energy f with respect to c_i and ϕ_α. Using the thermodynamical relation $e = f + sT$ it follows that

$$de = Tds + \sum_i \mu_i dc_i + \sum_\alpha r_\alpha d\phi_\alpha,$$
$$ds = \frac{1}{T} de - \sum_i \frac{\mu_i}{T} dc_i - \sum_\alpha \frac{r_\alpha}{T} d\phi_\alpha.$$

Interpreting s as function of $(e, \boldsymbol{c}, \boldsymbol{\phi})$ one gets

$$s_{,e} = \frac{1}{T}, \quad s_{,c_i} = \frac{-\mu_i}{T}, \quad s_{,\phi_\alpha} = \frac{-r_\alpha}{T}.$$

Knowing the free energy densities of the pure phases f_α, the total free energy f is obtained as a suitable interpolation of f_α.

The governing equations for the conserved order parameters e and $c_i, i = 1, \ldots, K$ are derived from the entropy functional in Equation (14.1)

$$\frac{\partial e}{\partial t} = -\nabla \cdot J_0 \qquad \text{(energy balance)}, \tag{14.3a}$$
$$\frac{\partial c_i}{\partial t} = -\nabla \cdot J_i \qquad \text{(mass balances, } i = 1, \ldots, K) \tag{14.3b}$$

and they are coupled to the evolution equations of the non-conserved order parameters $\phi_\alpha, \alpha = 1, \ldots, N$ via

$$\omega\varepsilon \frac{\partial \phi_\alpha}{\partial t} = \frac{\delta S}{\delta \phi_\alpha} - \lambda, \qquad \alpha = 1, \ldots, N, \tag{14.3c}$$

in such a way that the second law of thermodynamics is fulfilled in an appropriate local version. For the non-conserved phase-field variables ϕ_α, it is assumed that the system locally tends to maximize entropy, while, at the same time, concentration and energy is locally conserved. The variational derivative $\frac{\delta S}{\delta \phi_\alpha}$ of Equation(14.3c) gives

$$\omega\varepsilon \frac{\partial \phi_\alpha}{\partial t} = \varepsilon\big(\nabla \cdot a_{,\nabla\phi_\alpha} - a_{,\phi_\alpha}\big) - \frac{1}{\varepsilon} w_{,\phi_\alpha} - \frac{f_{,\phi_\alpha}}{T} - \lambda,$$

where $a_{,\phi_\alpha}, w_{,\phi_\alpha}, f_{,\phi_\alpha}$ and $a_{,\nabla\phi_\alpha}$ denote the derivatives of the energy contributions with respect to ϕ_α and $\nabla\phi_\alpha$, respectively. ω is a constant kinetic coefficient and λ is an appropriate Lagrange multiplier such that the constraint $\sum_{\alpha=1}^{N} \phi_\alpha = 1$ in Equation (14.2) is satisfied, i.e.

$$\lambda = \frac{1}{N} \sum_\alpha \left[\varepsilon \left(\nabla \cdot a_{,\nabla\phi_\alpha} - a_{,\phi_\alpha} \right) - \frac{1}{\varepsilon} w_{,\phi_\alpha} - \frac{f_{,\phi_\alpha}}{T} \right]. \tag{14.4}$$

The quantities on the right hand sides of the Equations (14.3a) and (14.3b) are the energy flux J_0 and fluxes $J_1, \ldots, J_K$ of the components $c_1, \ldots, c_K$. Appropriate expressions are

derived from generalized thermodynamic potentials $\frac{\delta S}{\delta e} = \frac{1}{T}$ and $\frac{\delta S}{\delta c_i} = \left(\frac{-\mu_i}{T}\right)$ driving the evolution. Appealing to non-equilibrium thermodynamics it is postulated that the fluxes are linear functions of the thermodynamic driving forces $\nabla\frac{\delta S}{\delta e}, \nabla\frac{\delta S}{\delta c_1}, \ldots, \nabla\frac{\delta S}{\delta c_K}$ to obtain

$$\begin{aligned} J_0 &= L_{00}(T, \boldsymbol{c}, \boldsymbol{\phi})\nabla\frac{\delta S}{\delta e} + \sum_{j=1}^{K} L_{0j}(T, \boldsymbol{c}, \boldsymbol{\phi})\nabla\frac{\delta S}{\delta c_j} \\ &= L_{00}(T, \boldsymbol{c}, \boldsymbol{\phi})\nabla\frac{1}{T} + \sum_{j=1}^{K} L_{0j}(T, \boldsymbol{c}, \boldsymbol{\phi})\nabla\frac{-\mu_j}{T}, \end{aligned} \tag{14.5a}$$

$$\begin{aligned} J_i &= L_{i0}(T, \boldsymbol{c}, \boldsymbol{\phi})\nabla\frac{\delta S}{\delta e} + \sum_{j=1}^{K} L_{ij}(T, \boldsymbol{c}, \boldsymbol{\phi})\nabla\frac{\delta S}{\delta c_j} \\ &= L_{i0}(T, \boldsymbol{c}, \boldsymbol{\phi})\nabla\frac{1}{T} + \sum_{j=1}^{K} L_{ij}(T, \boldsymbol{c}, \boldsymbol{\phi})\nabla\frac{-\mu_j}{T} \end{aligned} \tag{14.5b}$$

with mobility coefficients $(L_{ij})_{i,j=0,,\ldots,K}$ relating to heat and mass diffusion coefficients. To fulfill the constraint $\sum_{i=1}^{K} c_i = 1$ in Equation (14.2) during the evolution, is is required that $\sum_{i=1}^{K} L_{ij} = 0, j = 0, \ldots, K$ implying $\sum_{i=1}^{K} J_i = 0$ and hence $\partial_t\left(\sum_{i=1}^{K} c_i\right) = \nabla \cdot \left(\sum_{i=1}^{K} J_i\right) = 0$. Further, it is assumed that the L_{ij} are positive semi-definite and symmetric according to the Onsager relations. In Garcke, Nestler and Stinner (2002) it is shown that this condition leads to an entropy inequality ensuring positive local entropy production. Cross effects between mass and energy diffusion can be neglected by setting $L_{i0} = 0$ and $L_{0j} = 0$ for all $i, j \in \{1, \ldots, K\}$.

14.3 Free Energies

The diffuse interface model is capable of describing alloy systems with a very general class of multiphase multicomponent phase diagrams by specifying the free energies $f_\alpha(T, \boldsymbol{c})$. The model allows for systems with concave entropies $s_\alpha(e, \boldsymbol{c})$ in the pure phases corresponding to free energies $f_\alpha(T, \boldsymbol{c})$ being convex in c and concave in T. If $f(T, \boldsymbol{c}, \boldsymbol{\phi})$ is not convex in the variable c, the free energy needs to contain gradients of the concentrations as e.g. in a Cahn-Hilliard type model. Choosing the liquid phase to be the last component ϕ_N of the phase-field vector $\boldsymbol{\phi}$, the bulk free energies are defined for the individual phases by

$$f_\alpha(T, \boldsymbol{c}) = \sum_{i=1}^{K}\left(c_i L_i^\alpha \frac{T - T_i^\alpha}{T_i^\alpha} + k_B T c_i \ln(c_i)\right) - c_v T(\ln(T) - 1)$$

with $L_i^N = 0$ and $L_i^\alpha, i = 1, \ldots, K, \alpha = 1, \ldots, N-1$, being the latent heat per unit volume of the phase transition from phase α to the liquid phase and pure component i. Furthermore, $T_i^\alpha, i = 1, \ldots, K, \alpha = 1, \ldots, N-1$ is the melting temperature of the i-th component in the

phase α, c_v is the specific heat which is for simplicity assumed to be independent of $\boldsymbol{c}$ and $\boldsymbol{\phi}$; k_B is the Boltzmann constant. Then the total free energy density follows:

$$\begin{aligned} f(T,\boldsymbol{c},\boldsymbol{\phi}) := &\sum_{\alpha=1}^{M}\sum_{i=1}^{N}\Big(c_i L_i^\alpha \tfrac{T-T_i^\alpha}{T_i^\alpha} h(\phi_\alpha)\Big) \\ &+ \sum_{i=1}^{N}(k_\mathrm{B} T c_i \ln(c_i)) - c_v T\big(\ln(T)-1\big). \end{aligned} \tag{14.6}$$

With a suitable choice of the function $h(\boldsymbol{\phi})$ satisfying $h(0)=0$ and $h(1)=1$, e.g. $h(\phi_\alpha)=\phi_\alpha$ or $h(\phi_\alpha)=\phi_\alpha^2(3-2\phi_\alpha)$, the free energy density f is an interpolation of the individual free energy densities f_α. The entropy density $s(e,\boldsymbol{c},\boldsymbol{\phi})$, the inner energy density e as well as the chemical potentials μ_i follow from the free energy density in Equation (14.6):

$$s = -f_{,T} = -\sum_{\alpha=1}^{N}\sum_{i=1}^{K}\Big(c_i \tfrac{L_i^\alpha}{T_i^\alpha} h(\phi_\alpha)\Big) - \sum_{i=1}^{K}(k_\mathrm{B} c_i \ln(c_i)) + c_v \ln(T),$$

$$e = f + Ts = -\sum_{\alpha=1}^{N}\sum_{i=1}^{K}(c_i L_i^\alpha h(\phi_\alpha)) + c_v T. \tag{14.7a}$$

$$\mu_i(T,\boldsymbol{c},\boldsymbol{\phi}) = f_{,c_i}(T,\boldsymbol{c},\boldsymbol{\phi}) = \sum_{\alpha=1}^{N}\Big(L_i^\alpha \tfrac{T-T_i^\alpha}{T_i^\alpha} h(\phi_\alpha)\Big) + k_\mathrm{B} T(\ln(c_i)+1). \tag{14.7b}$$

Next, the terms modelling interfacial contributions to the free energy will be defined. In Garcke, Nestler and Stoth (1998, 1999b); Steinbach et al. (1996) it has been shown that gradient energies of the form

$$a(\boldsymbol{\phi},\nabla\boldsymbol{\phi}) = \sum_{\alpha,\beta=1,\alpha<\beta} A_{\alpha\beta}(\phi_\alpha\nabla\phi_\beta - \phi_\beta\nabla\phi_\alpha)$$

have very good properties with respect to calibrating parameters in the phase-field model to the surface terms in the sharp interface model. A choice that leads to isotropic surface terms is

$$a(\boldsymbol{\phi},\nabla\boldsymbol{\phi}) = \sum_{\alpha<\beta}\frac{\tilde{\gamma}_{\alpha\beta}}{\tilde{m}_{\alpha\beta}}\big|\phi_\alpha\nabla\phi_\beta - \phi_\beta\nabla\phi_\alpha\big|^2 \tag{14.8}$$

with constants $\tilde{\gamma}_{\alpha\beta}$ and $\tilde{m}_{\alpha\beta}$ that can be related to surface entropy densities $\gamma_{\alpha\beta}$ and kinetic coefficients $m_{\alpha\beta}$. In the case of surface energy anisotropy, the $\tilde{\gamma}_{\alpha\beta}$ parameters depend on the orientation of the interface. The antisymmetric formulation $\phi_\alpha\nabla\phi_\beta - \phi_\beta\nabla\phi_\alpha$ allows to treat the physics of each interface individually.

Expressions for the potential $w(\boldsymbol{\phi})$ can be formulated as direct extensions of the standard double well or double obstacle potential for solid-liquid phase-field models to a multi well $w_{st}(\boldsymbol{\phi})$ or multi obstacle potential $w_{ob}(\boldsymbol{\phi})$ for the multi phase model:

$$w_{st}(\boldsymbol{\phi}) = 9\sum_{\alpha<\beta}\tilde{m}_{\alpha\beta}\tilde{\gamma}_{\alpha\beta}\phi_\alpha^2\phi_\beta^2 \quad\text{and}\quad w_{ob}(\boldsymbol{\phi}) = \frac{16}{\pi}\sum_{\alpha<\beta}\tilde{m}_{\alpha\beta}\tilde{\gamma}_{\alpha\beta}\phi_\alpha\phi_\beta. \tag{14.9}$$

By numerical experiments comparing different choices for the potential $w(\boldsymbol{\phi})$, it is found that the multi obstacle potential with additional higher order variants

$$\tilde{w}_{ob}(\boldsymbol{\phi}) = w_{ob}(\boldsymbol{\phi}) + \sum_{\alpha<\beta<\delta} \gamma_{\alpha\beta\delta}\phi_\alpha\phi_\beta\phi_\delta$$

yields the best calibration properties. It is generally difficult in multi phase-field models to compute the surface free energy densities (or surface entropy densities). In studies by Garcke, Nestler and Stoth (1999a) free energies for phase-field methods with good calibration properties have been developed. This means that for experimentally given surface free energies one can calibrate the parameters in the free energies of the phase-field model in such a way that the sharp interface limit is defined via the given surface tensions. Another advantage of using an obstacle type potential for numerical simulations is that the potentials $w_{ob}(\boldsymbol{\phi})$ or $\tilde{w}_{ob}(\boldsymbol{\phi})$ are defined to be infinity whenever $\boldsymbol{\phi}$ is not on the Gibbs-Simplex. Therefore, the equations for the phase-fields $\phi_\alpha, \alpha = 1, \ldots, N$ only need to be solved in the region of the diffuse interface layer. It is referred to Garcke, Nestler and Stoth (1999a,b) for a further discussion of the properties of the surface terms.

To complete the explicit definitions of quantities in the diffuse interface model, an example for the mobility matrix $(L_{ij})_{i,j=0,\ldots,N}$ is given defining heat and mass diffusion as well as cross effects between them. By assuming that the mobilities of the pure components are linear in c_i and by referring to Garcke, Nestler and Stinner (2002) the following expressions are obtained

$$L_{ij} = D(T, \boldsymbol{c}, \boldsymbol{\phi})c_i(\delta_{ij} - c_j), \tag{14.10}$$

$$L_{0j} = -\sum_{i,\alpha} D(T, \boldsymbol{c}, \boldsymbol{\phi})c_j(\delta_{ij} - c_i)h(\phi_\alpha)L_i^\alpha, \tag{14.11}$$

$$L_{00} = k(T, \boldsymbol{c}, \boldsymbol{\phi})T^2 + \sum_{i,j,\alpha,\beta} D(T, \boldsymbol{c}, \boldsymbol{\phi})h(\phi_\alpha)L_i^\alpha c_j(\delta_{ij} - c_i)h(\phi_\beta)L_j^\beta, \tag{14.12}$$

where $D(T, \boldsymbol{c}, \boldsymbol{\phi})$ and $k(T, \boldsymbol{c}, \boldsymbol{\phi})$ contain mass and heat diffusion coefficients and δ_{ij} denotes the Kronecker delta.

14.4 Numerical Simulations

Inserting the relations for λ, J_0, J_i in Equations (14.4,14.5a,14.5b), the free energies f, a, w in Equations (14.6,14.8,14.9), the mobility matrix (L_{ij}) in Equations (14.10,14.11,14.12) and the resulting derivatives for e, μ_i in Equations (14.7a, 14.7b) into the governing equations in Equations (14.3a,14.3b,14.3c), a full set of evolution equations for the inner energy, the concentrations and the phase-fields is set up and discretized. Numerical simulations of the motion of multiple interfaces in grain structures, of solidification processes and phase transitions in multi component alloy systems are performed. For simulating microstructure evolutions in large domains at acceptable computation times, two different strategies are used: A 3D parallel simulator based on a heterogeneous network and on a server-client mechanism is set up for parallel solving of the partial differential equations with a finite difference discretization and

an explicit time scheme. Alternatively, an adaptive finite element method with a semi-implicit time discretization is applied to solve the equations. Diffuse interface simulations require that the spatial resolution of the numerical method is greater than the thickness of the diffusive phase boundary layer. The interfacial thickness itself must be less than the characteristic scale of the growing microstructure. In this case, a nonuniform grid with adaptive refinement can dramatically reduce the use of computational resources compared to a uniform grid with the same spatial resolution. Both approaches may converge to a hybrid solution at some future stage.

14.4.1 Grain Growth and Coarsening

The first simulation in Figure 14.1 is motivated by an experiment of heteroepitaxial thin film growth of a cubic tricrystalline aluminum grain structure on a silicon substrate, described in Dahmen and Thangaraj (1993). According to the experimental setup, the focus lies on a tricrystalline grain formation with three allowed orientational variants. The variants are rotated about a common <001> axis by 30° with respect to each other. Two superimposed cubic grains with a relative rotation of 30° between their crystallographic orientation exhibit eight symmetry/mirror axes. The symmetry/mirror axes are preferred directions for grain boundaries to be formed, because in these directions the boundaries are in states of minimal energy. This can be explained using the criterion of symmetry dictated-extrema, Cahn and Kalonji (1994). Therefore, an eightfold convex and crystalline (facetted) surface energy anisotropy is formulated having a typical cusp-like structure at the eight preferred directions (see Garcke, Nestler and Stoth (1999b) for the anisotropy formulation).

As in experimental observations, the grain boundaries in polycrystalline structures are forced by a minimization of energy criterion to evolve at certain symmetry conditions. Force balance laws lead to grain configurations with adjacent triple junctions which must always belong to different symmetry classes and hence adjust at different angle conditions. The evolution of the triple junctions is driven by the classical Young's law. This law relates the surface energies meeting at the junctions to the angles formed at the junction. In the case of anisotropic surface energies, in particular crystalline (facetted) energies, additional shear forces in tangential direction to the grain boundaries occur in the Young's equation. A more detailed description of the crystalline modification of Young's law was first derived in Garcke and Nestler (2000).

In numerical computations, triple junctions and the influence of surface energy anisotropy on the angle condition at the triple junction are investigated. In accordance with the classical equilibrium force balance law by Young with shear forces due to surface energy anisotropy, angle conditions differing from the equal 120° case are obtained as a result of additional torque terms in this anisotropic force balance equation. Wetting behavior that occurs in physical systems, if the surface energies violate the stability condition $\gamma_{ij} \leq \gamma_{ik} + \gamma_{kj}$ can also be recovered.

The simulation in Figure 14.2 shows the process of two-dimensional grain growth and coarsening in a system of multiple grains. In this context, the components ϕ_α of the multiple order parameter model describe different orientational variants in a crystalline material. In a system where all the surface energies are equal as in Figure 14.2, all triple junctions have a 120° angle condition. Characteristic features of the von Neumann law can be observed

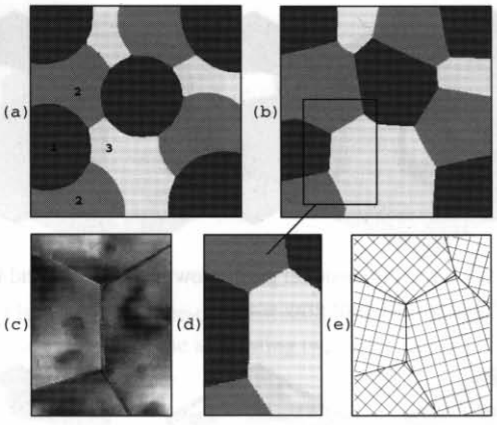

Figure 14.1: Simulation (a,b,d) and experiment (c) of a tricrystalline microstructure with three grains (shown in different gray tones) rotated by 30° about a common <001> axis with respect to each other, a), b), d) computed grain growth, c) grain boundaries reconstructed from experimental observations by Dahmen and Thangaraj (1993), e) schematic drawing of a cubic tricrystalline grain structure.

postulating that grains with less than six neighbors shrink, grains with more than six neighbors grow and six–sided grains keep their area in time. A region which shrinks is marked by a cross whereas a region which keeps the area is marked by a circle.

Next, the phase-field model is applied to three-dimensional grain growth phenomena in an isotropic and anisotropic grain system in Figures 14.3 and 14.4, respectively. The simulations are performed with five order parameters. For the computation in Figure 14.4, a crystalline hexagonal anisotropy with grains of different crystallographic orientations is chosen. The evolution of the grain boundaries support the fact that facets form in certain preferred directions and that anisotropy changes the equilibrium angle condition of 120° at triple junctions.

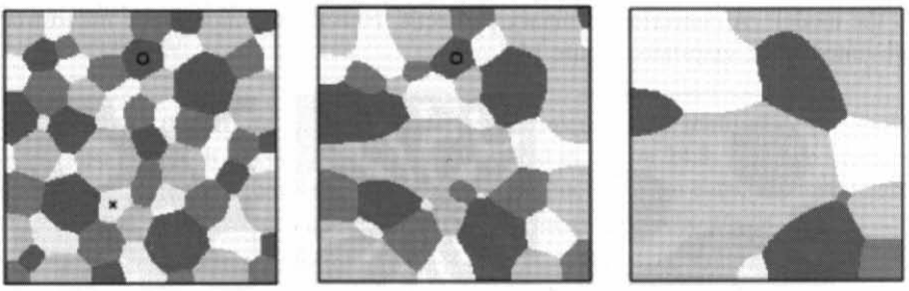

Figure 14.2: Two-dimensional grain growth and coarsening in a system of four grains (shown in different gray tones) with equal surface energies illustrating characteristic features of the von Neumann law: The grain marked by a circle has six corners and remains stable in size, the grain indicated by a cross has five corners and the tendency to shrink.

14.4.2 Multicomponent Multiphase Solidification

The objective of this section is to show the utility of the diffuse interface model to simulate a wide variety of realistic growth structures and morphologies in multicomponent multiphase systems as reported in Kurz and Fisher (1992); Sahm and Kurz (1975); Akamatsu and Faivre (2000). To describe the phase transitions and solidification processes in metallic alloys, the

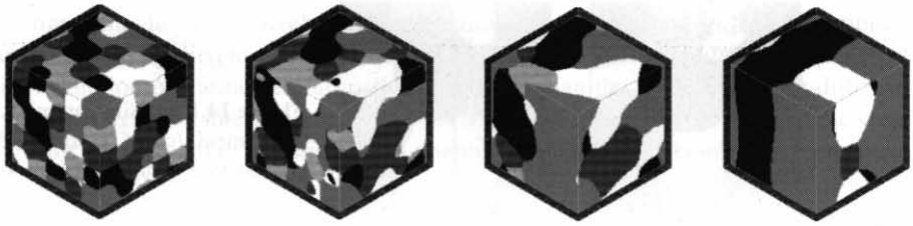

Figure 14.3: Phase-field simulation of three-dimensional grain growth with equal and isotropic surface energies. The grains are colored by different gray scales.

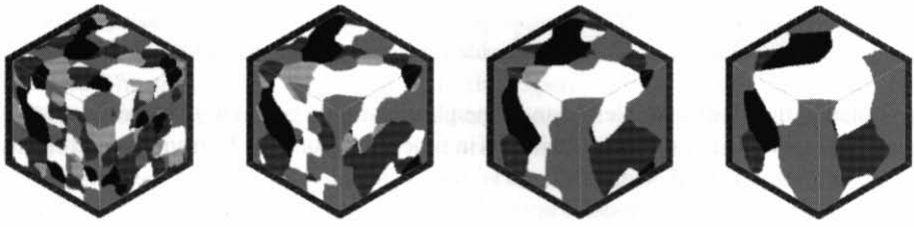

Figure 14.4: Phase-field simulation of three-dimensional grain growth with crystalline (facetted) hexagonal surface energies and grains of different orientation.

specific physical parameters and the phase diagram are taken into account via the free energies in the model. A collection of binary peritectic, eutectic and monotectic microstructures is presented in the snapshots, Figure 14.5.

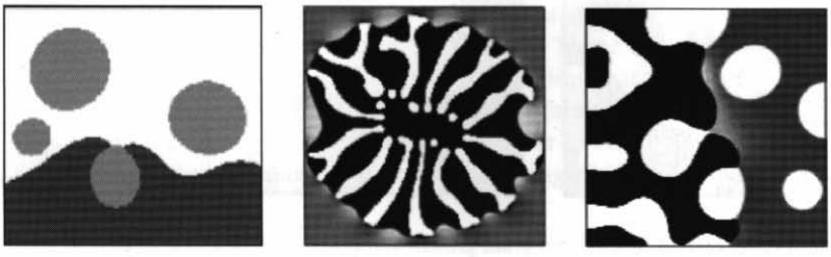

Figure 14.5: Snapshots of a simulated binary alloy solidification of a peritectic (left), a eutectic (middle) and monotectic system (right). The growing bulk phases are illustrated in white and black. The concentration profile in the undercooled melt with depleted and enriched regions is shown in continuously varying gray scale.

Examples for three-dimensional binary eutectic alloy structures are displayed in Figures 14.6 and 14.7. Once the parent liquid phase (metallic melt) is cooled below the eutectic temperature, the liquid phase L transforms into two new solid phases α and β via a eutectic reaction: $L \rightarrow \alpha + \beta$. The phase-field simulations were carried out taking a symmetric phase diagram and periodic boundary conditions.

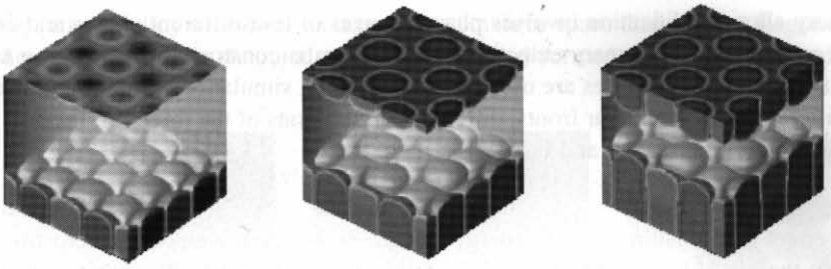

Figure 14.6: Three-dimensional simulation of a binary eutectic alloy establishing a regular rod-like structure of the alternating two solid phases growing into the undercooled melt (transparent gray).

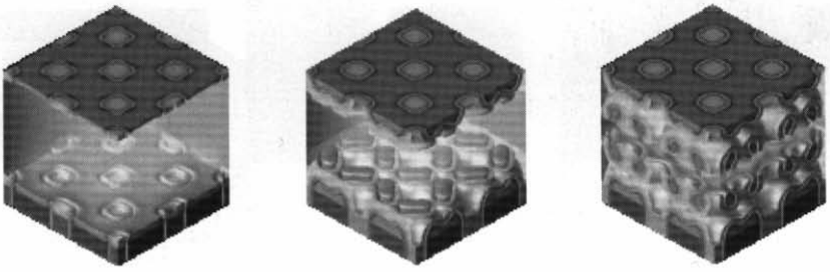

Figure 14.7: Irregular three-dimensional growth mode of a binary eutectic due to the antisymmetric initial phase configuration differing from the symmetric eutectic phase diagram chosen for the simulation.

An application of the diffuse interface modelling technique to the multi-scale phenomena of competitive evolution of eutectic grains is illustrated in Figure 14.8. The two involved length scales are the grain structure on a large scale and the finer lamellar eutectic substructure. The simulation was set up with different anisotropies for the two eutectic grains.

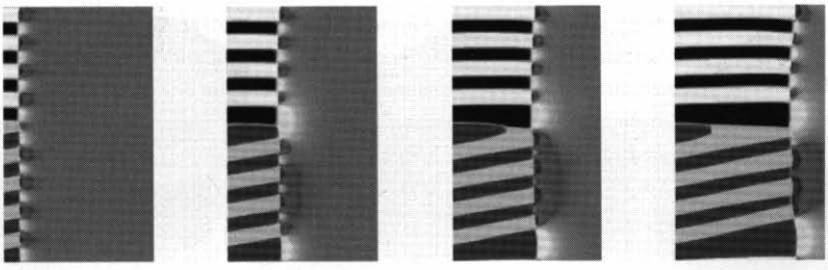

Figure 14.8: Two eutectic grains (white/black and light/dark-gray) of a binary alloy with different crystal orientations growing into the melt (continuous gray scale). The images visualize the phase evolution and concentration profiles of the alloy composition in the liquid ahead of the growing solid phases at different time steps.

Ternary alloy solidification involves phase changes of four different phases and diffusion of three components. A ternary eutectic phase diagram is constructed by common tangents and the according free energies are used for the following simulations. Aiming to investigate the stability of ternary lamellar fronts, different permutations of the three solid phases α, β, γ are considered in Figure 14.9 and Figure 14.10.

The effect of crystalline surface energy anisotropy on ternary eutectic microstructures is studied in the phase-field simulations of Figures 14.11 and 14.12. The anisotropy leads to tilted growth typically observed in experiments. A phase shift within the lamellae occurs for crystal orientations aligned in the growth direction.

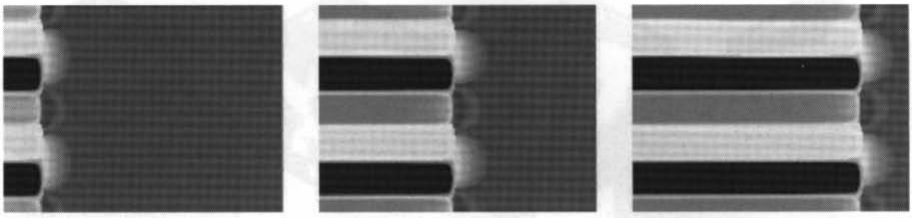

Figure 14.9: Ternary eutectic lamellae with a configuration α (gray), β (black), γ (white), showing the concentration of one of the components in the melt (continuous gray scale) at three different times.

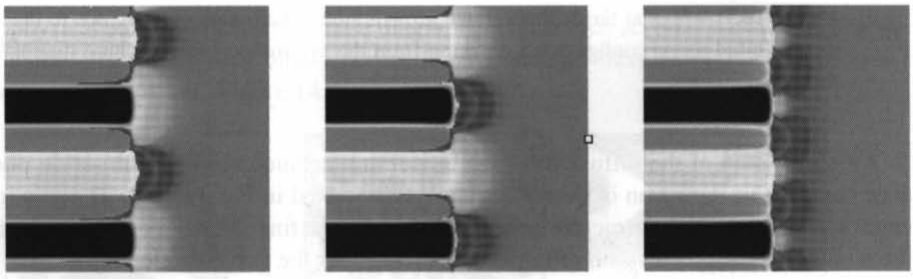

Figure 14.10: Ternary eutectic lamellae with a configuration α (gray), β (black), α (gray), γ (white). The three pictures illuminate the concentration fields (continuous gray scale) ahead of the solid front for all three components of the $A - B - C$ alloy at a medium time step.

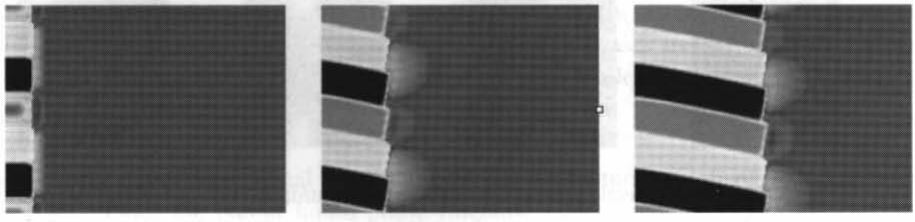

Figure 14.11: Tilted solidification front in a ternary eutectic alloy with three solidifying solids (gray, black, white) as a result of the influence of surface energy anisotropy.

Finally, ternary alloy solidification is computed in three space dimensions. Regular lamellae of the α, β, γ solids in diagonal space direction are formed for the initial condition in Figure 14.13.

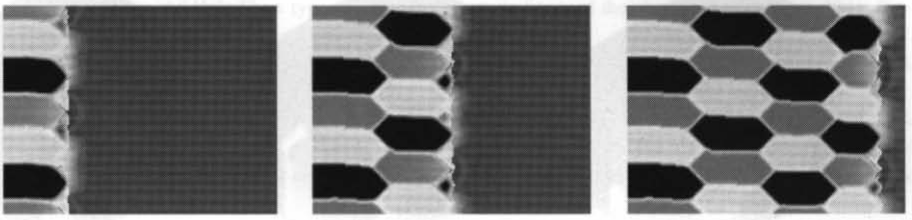

Figure 14.12: Phase shifts in ternary eutectic solid phases with a fourfold crystalline anisotropy.

Figure 14.13: Three-dimensional computation of a ternary eutectic alloy with three different solid phases (gray, black, white) evolving with steady state lamellar growth behavior in diagonal space direction.

All three solid phases grow from the liquid phase. While simultaneously growing, the solid phases mutually enhance each other's growth conditions as they reject opposite components of the alloy into the liquid. This leads to the establishment of a steady regular hexagonal shape in Fig 14.14 with phase boundaries having isotropic surface energies.

Figure 14.14: The dynamic solidification process of ternary eutectic hexagonal rods corresponding to three different times.

In a subsequent computation the phase evolution was simulated taking crystal anisotropy and differently rotated solid particles into account, Figure 14.15.

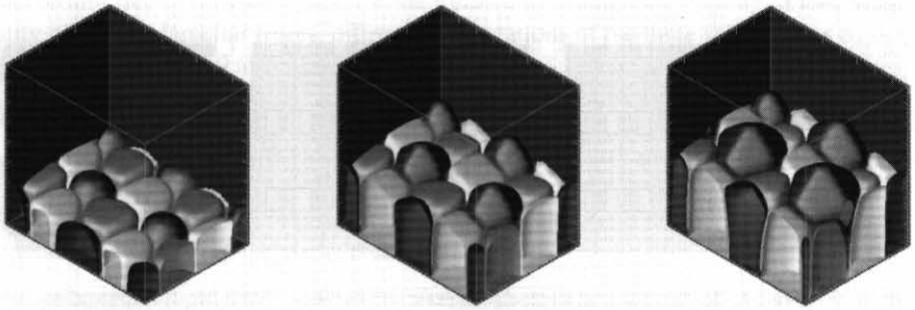

Figure 14.15: The influence of crystalline surface energies on the evolution of phase boundaries in a phase-field simulation of ternary eutectic phase transitions forming strong facets in the preferred growth directions.

14.5 Outlook

A thermodynamically consistent diffuse interface model (phase-field model) has been developed describing non-isothermal solidification in alloy systems with multiple components and phases. The new model was discretized and two- and three-dimensional simulations of phase transitions, of solidification processes, of complex microstructure formations and of interfacial motion in polycrystalline grain structures are performed. Based on these results, it is intended to apply the phase-field simulations to model complex multiscale growth phenomena involving different length (and time) scales. Examples are the growth of eutectic colonies resulting from small amounts of ternary impurities and dendritic networks with interdendritic eutectic substructures. In order to quantitatively describe phase transformations and solidification processes in multi-component alloys, it is planned to incorporate specific phase diagrams into the phase-field model via the free energies by linking the governing equations to a thermodynamics data base. Another challenge for future work is to include convection into the phase-field model, to investigate the interaction of different physical fields and their effect on the microstructure evolution.

Acknowledgements

The author gratefully thanks Harald Garcke and his group for collaboration over many years. The financial support through the German Research Foundation within the two priority research programs: Multiscale problems (1095) and phase transitions in multicomponent melts (1120) is gratefully acknowledged.

References

Akamatsu, S. and Faivre, G., 2000. Traveling wavers, Two-phase fingers, and eutectic colonies in thin-sample directional solidification of ternary eutectic alloy, Phys. Rev. E, Vol. **61**, Nr. 4, 3757.

Caginalp, G., 1989. Stefan and Hele Shaw type models as asymptotic limits of the phase-field equations, Phys. Rev. A **39**, No. 11, pp. 5887–5896.

Caginalp, G. and Fife, P. C., 1988. Dynamics of layered interfaces arising from phase boundaries, SIAM J. Appl. Math. **48**, 506–518.

Caginalp, G., Xie, W., 1998. An analysis of phase-field alloys and transition layers, Arch. Rat. Mech. Anal. **142**, 293–329.

Cahn, J. W. and Hilliard, J. E., 1958. Free energy of a nonuniform system I. Interfacial free energy, J. Chem. Phys. **28**, 258–267.

Cahn, J. W. and Kalonji, G., 1994. Symmetries of grain boundary trijunctions, J. Phys. Chem. Solids **55**, 1017–1022.

Chalmers B., 1977. Principles of solidification, Krieger Pub.

Chen, L. Q. and Yang, W., 1994. Computer simulation of the domain dynamics of a quenched system with a large number of non-conserved order parameters: the grain–growth kinetics, Phys. Rev. B **50**, No. 21, pp. 15752–15756.

Dahmen, U. and Thangaraj, N., 1993. Grain boundaries in mazed multicrystal microstructures of Al, Mat. Sci. Forum **126–128**, 45–54.

Fan, D. N. and Chen, L. Q., 1997. Diffuse-Interface Description of Grain Boundary Motion, Philosophical Magazine Letters **75**, pp. 187–196.

Fried, E. and Gurtin, M. E., 1994. Dynamic solid-solid transitions with phase characterized by an order parameter, Physica D **72**, pp. 287–308.

Garcke, H. and Nestler, B., 2000. A mathematical model for grain growth in thin metallic films, Math. Models and Methods in Applied Sciences **10**, No. 6, 895–921.

Garcke, H., Nestler, B., Stinner, B., 2002. A diffuse interface model for alloys with multiple components and phases, submitted to SIAM J. Appl. Math.

Garcke, H., Nestler, B. and Stoth, B., 1998. On anisotropic order parameter models for multi–phase systems and their sharp interface limits, Physica D **115**, 87–108.

Garcke, H., Nestler, B. and Stoth, B., 1999. A Multi Phase Field Concept: Numerical Simulations of Moving Phase Boundaries and Multiple Junctions, SIAM J. Appl. Math., Vol. **60**, No. 1, 295–315.

Garcke, H., Nestler, B. and Stoth, B., 1999. Anisotropy in multi-phase systems: A phase field approach, Interfaces and Free Boundaries 1, pp. 175–198.

Haasen, P., 1994. Physikalische Metallkunde, Springer, 3. ed. 1994.

Halperin, P. I., Hohenberg, P. C. and Ma, S.-K., 1974. Renormalization group methods for critical dynamics I. Recursion relations and effects of energy conservation, Phys. Rev. B **10**, 139–153.

Karma, A., 2001. Phys. Rev. Lett. **87**, 115701.

Karma, A. and Rappel, 1998. Phys. Rev. E **57**, 4323.

Kurz, W. and Fisher, D. J., 1992. Fundamentals of Solidification, Trans Tech, Aedermannsdorf, Switzerland.

Landau, L. D. and Ginzburg, V. I., 1950. K teorii sverkhrovodimosti, Zh. Eksp. Teor. Fiz 20 (1950) 1064, English translation 1965: On the theory of superconductivity, in Collected papers of L. D. Landau, ed. D. ter Haar, Pergamon, Oxford, 626–633.

Langer, J. S., 1986. Models of pattern formation in first–order phase transitions, Directions in Condensed Matter Physics, World Scientific, Singapore, 165–186.

Lowengrub, J., Truskinovsky, L., 1998. Quasi-incompressible Cahn-Hilliard fluids and topological transitions, Proc. Roy. Soc. London A **454**, pp. 2617–2654.

Nestler, B., Wheeler, A. A., 1998. Anisotropic multi-phase-field model: Interfaces and junctions, Phys. Rev. E **57**, No. 3, 2602–2609.

Nestler, B. and Wheeler, A. A., 2000. A Multi-phase-field Model of Eutectic and Peritectic Alloys: Numerical Simulation of Growth Structures, Physica D **138**, 114–133.

Nestler, B., Wheeler, A. A. and Garcke, H., Modelling of microstructure formation and interface dynamics, J. Comp. Mater. Sci. (to appear).

Nestler, B., Wheeler, A. A., Ratke, L. and Stöcker, C., 2000. Phase-Field Model for Solidification of a Monotectic alloy with convection, Physica D **141**, 133–154.

Penrose, O. and Fife, P. C., 1990. Thermodynamically consistent models of phase field type for the kinetics of phase transition, Physica D 43, 44–62.

Plapp, M. and Karma, A., 2002. Eutectic colony formation: A phase-field study, Phys. Rev. E 66, 061608.

Kurz, W. and Sahm, P. R., 1975. Gerichtet erstarrte eutektische Werkstoffe, Reine und angewandte Metallkunde in Einzeldarstellungen, Bd. 25, Springer-Verlag Berlin Heidelberg New York 1975.

Steinbach, I., Pezolla, F., Nestler, B., Seeßelberg, M., Prieler, R., Schmitz G. J., and Rezende, J. L. L., 1996. A phase field concept for multi phase systems, Physica D **94**, pp. 35–147.

Sternberg, P., 1991. Vector–valued local minimizers of nonconvex variational problems, Rocky Mt. J. Math. **21**, No. 2, pp. 799–807.

Tiaden, J., Nestler, B., Diepers, H. J., Steinbach, I., 1998. The multiphase-field model with an integrated concept for modelling solute diffusion, Physica D **115**, 73–86.

van der Waals, J. D., 1893. The thermodynamic theory of capillarity under the hypothesis of a continuous variation of density (translation of Dutch title): Konink. Akad. Weten. Amsterdam, Vol. 1, No. 8 (1893), English translation: J. S. Rowlinson, J. Stat. Phys. **20**, 197–244.

Visintin, A., 1996. Models of Phase Transition, Birkhäuser, Boston.

Wang, S.-L., Sekerka, R. F., Wheeler, A. A., Murray, B. T., Coriell, S. R., Braun, R. J. and McFadden, G. B., 1993. Thermodynamically–consistent phase–field models for solidification, Physica D **69**, 189–200.

Wheeler, A. A., McFadden, G. B. and Boettinger, W. J., 1996. Phase–field model for solidification of a eutectic alloy, Proc. Roy. Soc. Lond. A **452**, pp. 495–525.